Sensors & Actuators: B. Chemical 430 (2025) 137401

Contents lists available at ScienceDirect

Sensors and Actuators: B. Chemical

journal homepage: www.elsevier.com/locate/snb

Ultra-large stokes-shifted NIR fluorescent probes for the diagnosis and treatment of rheumatoid arthritis *via* metal-free tracking of carbon monoxide

Wenping Dong [a], Mo Ma [a,b], Jingkang Li [a], Dejiang Gao [a], Pinyi Ma [a,*], Daqian Song [a,*]

[a] College of Chemistry, Jilin Province Research Center for Engineering and Technology of Spectral Analytical Instruments, Jilin University, Qianjin Street 2699, Changchun 130012, China
[b] School of Pharmacy, Jilin University, Qianjin Street 2699, Changchun 130012, China

ARTICLE INFO

Keywords:
Carbon monoxide (CO)
Fluorescent probe
Rheumatoid arthritis
Early diagnosis
In vivo imaging

ABSTRACT

Early diagnosis of rheumatoid arthritis (RA) is essential for preventing disease progression and improving prognosis. This study proposes the use of carbon monoxide (CO) as a potential biomarker for RA. Two fluorophores, HM-OH and DHM-OH, were designed and synthesized, using DHM-OH due to its superior spectroscopic properties. The combination of DHM-OH with allyl bromide produced the fluorescent probe DHM-CO, which had a large Stokes shift (302 nm) and a long emission wavelength (882 nm). DHM-CO enabled metal-free catalytic detection of CO. The probe was demonstrated to have excellent water solubility, photostability, and high sensitivity to CO; therefore, it could selectively respond to CO without interference from other substances. The limit of detection of the probe in the detection of CORM-3, a CO precursor, was as low as 0.027 μM. DHM-CO was successfully used for the imaging of endogenous and exogenous CO in A549 cells. It was also successful in the tracking of CO in RA models, revealing that the CO concentrations in RA joints were significantly higher compared to that in normal joints. Additionally, the therapeutic effect of methotrexate (MTX) on RA was verified. This study introduces the first imaging of CO in RA, offering a valuable tool for early diagnosis and treatment of RA.

1. Introduction

Carbon monoxide (CO) has historically been regarded as a toxic and dangerous gas due to its strong affinity for hemoglobin [1,2]. High concentrations can cause poisoning and endanger tissues such as the brain, heart, liver, kidneys, and lungs [3]. Despite its toxicity, CO is a key gaseous signaling molecule produced in the body through hemoglobin catabolism mediated by hemoglobin oxygenases (HO-1 and HO-2) [4]. Recent research has shown that endogenous CO is involved in various physiological and pathological activities, including neurotransmission and anti-apoptosis [5]. Additionally, oxidative stress can increase endogenous CO levels to scavenge free radicals, reduce oxides, and protect cells [6]. However, the pathological mechanisms of CO in organisms remain unknown [7–10]. Therefore, the ability to detect endogenous CO *in vivo* is crucial for early disease diagnosis and assessing inflammatory progression.

Rheumatoid arthritis (RA) is a chronic autoimmune disease that causes joint pain, swelling, and dysfunction. It remains incurable and persistent throughout a lifetime [11–13]. Oxidative stress plays a key role in RA and is involved in inflammation and joint damage. Elevated HO-1 levels in RA patients increase CO production, which in turn affects inflammation and RA severity [14–17]. Currently, studies diagnosing RA by detecting CO levels have not been reported, and yet CO could serve as a potential biomarker for RA. Traditional CO probes often use transition metal-mediated carbonylation reactions or Pd⁰-mediated Tsuji-Trost reactions, which can be cytotoxic [3,6,18–20]. Conventional imaging techniques such as computed tomography (CT), ultrasound, and magnetic resonance imaging (MRI) are used clinically to diagnose RA [21]; however, these techniques suffer from their low sensitivity, poor spatial and temporal resolution, and potential radiological risks. Hence, there is a critical need for a safe and effective method to detect CO in RA diagnosis and treatment.

Fluorescent sensors are increasingly used for disease diagnosis due to their non-invasiveness, high sensitivity, and real-time detection

* Corresponding authors.
E-mail addresses: mapinyi@jlu.edu.cn (P. Ma), songdq@jlu.edu.cn (D. Song).

https://doi.org/10.1016/j.snb.2025.137401
Received 3 September 2024; Received in revised form 4 January 2025; Accepted 5 February 2025
Available online 6 February 2025

capabilities. Near-infrared (NIR) fluorescent probes are favorable among researchers due to their low background interference, minimal photodamage, and high tissue penetration [22–27]. However, most fluorescent probes emit light in the 650–900 nm wavelength range with a small Stokes shift [3,28–30], which can interfere with the analysis of biological autofluorescence and diminish imaging penetrability. The autofluorescence can impair the accuracy and sensitivity of the detection [31–34], which highlights the need for fluorescent probes with long emission wavelengths and large Stokes shifts.

In this work, two fluorophores, HM-OH and DHM-OH, were designed, and their photophysical properties were compared. By extending the π-conjugation system, the emission wavelength and Stokes shift of the fluorophores were effectively increased. DHM-OH was selected for further study. A novel near-infrared fluorescent probe, DHM-CO, was designed and synthesized based on DHM-OH. The probe consisted of DHM-OH (the reporter unit) and an allyl group (the responsive unit). The evaluation of water solubility, photostability, and sensitivity of DHM-CO to CO, as well as its selectivity over other bioactive molecules, were conducted. Additionally, the probe's ability to detect exogenous and endogenous CO in cellular models and to visualize CO levels in RA animal models were investigated.

2. Experimental procedure

2.1. Organic synthesis

Scheme 1 illustrates the synthetic route of HM-OH and DHM-CO. The detailed synthesis procedures for Compound 1 and HM-OH can be found in the Supplementary Material. Figs. S1-S3 depict ^{1}H NMR, ^{13}C NMR and MS of HM-OH.

2.1.1. Synthesis of DHM-OH

Compound 1 (0.598 g, 2 mmol) and 4-tert-butyl-2,6-diformylphenol (0.206 g, 1 mmol) were dissolved in 20 mL of anhydrous ethanol. After a drop of piperidine was added as a catalyst, the mixture was refluxed at 85 °C for 12 h. The resulting brown solid was obtained via vacuum distillation. The crude product was purified by column chromatography (CH_2Cl_2/CH_3OH = 50:1), which yielded a tan solid with a 90 % yield. ^{1}H NMR (300 MHz, DMSO-d_6) δ 8.91 (d, J = 14.5 Hz, 2H), 8.65 (d, J = 9.3 Hz, 2H), 8.48 (d, J = 9.3 Hz, 2H), 8.33 (dd, J = 11.8, 2.1 Hz, 4H), 8.19 (dd, 2H), 8.03 (t, J = 7.9 Hz, 2H), 7.77 (t, J = 7.5 Hz, 2H), 7.61 (s, 2H), 7.31 (d, J = 4.5 Hz, 1H), 4.87 (q, J = 6.9 Hz, 4H), 1.63 (t, J = 7.1 Hz, 6H), 1.34 (s, 9H) (Fig. S4). ^{13}C NMR (75 MHz, DMSO-d_6) δ 157.19, 149.78, 141.29, 138.63, 137.05, 134.49, 134.18, 130.43, 127.89, 127.16, 126.35, 120.38, 118.43, 112.57, 46.14, 34.00, 31.67, 13.45 (Fig. S5). MS (m/z) for $C_{36}H_{38}N_2O^{+}$ [M] $^{+}$ calcd: 257.1487; found: 257.1487 (Fig. S6).

2.1.2. Synthesis of the probe DHM-CO

DHM-OH (0.230 g, 0.3 mmol) and Cs_2CO_3 (0.097 g, 0.3 mmol) were dissolved in 10 mL of CH_3CN. Then, 0.3 mL of allyl bromide was added dropwise into the flask, and the mixture was refluxed at 85 °C for 12 h. After vacuum distillation, the crude product was purified by column chromatography (CH_2Cl_2/CH_3OH=30:1), which yielded a yellow solid with a 20 % yield. ^{1}H NMR (600 MHz, DMSO-d_6) δ 9.19 (d, J = 8.9 Hz, 2H), 8.67 (d, J = 9.1 Hz, 2H), 8.57 (d, J = 8.9 Hz, 2H), 8.46 (dd, J = 8.2, 1.3 Hz, 2H), 8.27 (ddd, J = 8.7, 7.1, 1.4 Hz, 2H), 8.18 – 8.15 (m, 4H), 8.04 (d, J = 5.7 Hz, 2H), 8.02 (d, 2H), 6.25 – 6.19 (m, 1H), 5.53 (dq, J = 17.2, 1.5 Hz, 1H), 5.33 (dd, J = 10.5, 1.4 Hz, 1H), 5.21 (q, J = 7.1 Hz, 4H), 4.61 (d, J = 5.5 Hz, 2H), 1.61 (t, J = 7.2 Hz, 6H), 1.48 (s, 9H) (Fig. S7). ^{13}C NMR (151 MHz, DMSO-d_6, DPTE-Q) δ 156.12, 155.75, 148.33, 145.68, 141.95, 138.57, 136.02, 134.12, 131.03, 129.73, 129.22, 122.50, 121.58, 119.58, 119.00, 76.97, 47.73, 31.59, 31.02, 14.57. (Fig. S8). MS (m/z) for $C_{39}H_{42}N_2O^{+}$ [M] $^{+}$ calcd: 277.1643; found: 277.1649 (Fig. S9).

2.2. Preparation of samples for spectrophotometric analysis

In the preparation of samples for spectrophotometric analysis, a 1 mM stock solution was first prepared by dissolving the probe DHM-CO in dimethyl sulfoxide (DMSO). A 1 mL sample containing 10 μM DHM-CO, analyte at a specified concentration, DMSO, and PBS (10 mM, pH 7.4) was analyzed using a fluorescence spectrometer and a UV–vis spectrophotometer. The reaction mixture was incubated at 37 °C in PBS buffer (10 mM, pH 7.4) containing 50 % (v/v) DMSO for 60 min, unless stated otherwise, before detection.

2.3. Imaging of cells

2.3.1. Imaging of exogenous CO

Time-dependent imaging experiment: Six groups of A549 cells were incubated with 10 μM DHM-CO. After the addition of 50 μM CORM-3, the cells were imaged at various time points.

Concentration-dependent imaging experiment: Five groups of A549 cells were incubated with 10 μM DHM-CO, and after being treated with CORM-3 at different concentrations (0, 10, 25, 50, and 100 μM), they were subjected to imaging.

2.3.2. Imaging of endogenous CO

A549 cells were divided into three groups: (1) Control group: A549 cells were incubated with 10 μM DHM-CO for 1 h and then directly subjected to imaging; (2) LPS-treated group: A549 cells were treated with lipopolysaccharide (LPS) (0.1 mg/mL, 200 μL) for 3 h, incubated with 10 μM DHM-CO for 1 h, and then washed three times with PBS (10 mM, pH 7.4) before imaging; and (3) LPS and PG-treated group: A549 cells were first treated with LPS (0.1 mg/mL, 200 μL) for 3 h, followed by penicillin G sodium salt (PG, 0.1 mg/mL, 200 μL) for another 3 h, and after being washed three times with PBS (10 mM, pH 7.4), they were incubated with 10 μM DHM-CO for 1 h before imaging.

The cell imaging experiments were conducted using an Olympus FV1000 laser scanning confocal microscope at an excitation wavelength of 580 nm.

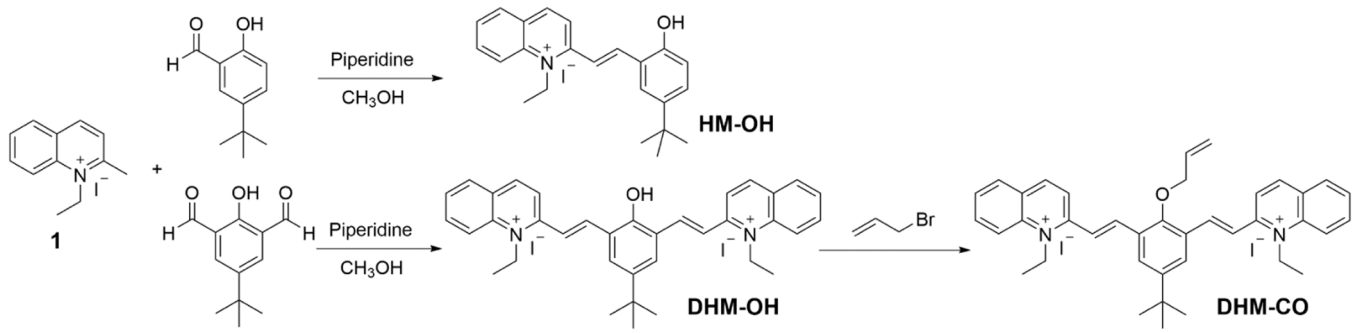

Scheme 1. Synthetic route of HM-OH and DHM-CO.

2.4. Imaging of mouse models

BALB/c mice (5–6 weeks old) were procured from BEIJING HFK BIOSCIENCE Co., LTD. (Beijing, China). All animal experiments were performed in accordance with the guidelines set by the Regional Ethics Committee for Animal Experiments established by the Jilin University Institutional Animal Care and Use Committee (No. SY202306031).

2.4.1. Establishment of rheumatoid arthritis (RA) mouse model

A rheumatoid arthritis (RA) mouse model was created by injecting λ-carrageenan (5 mg/mL, 50 μL) into the hind limbs of mice every three days for two consecutive weeks.

2.4.2. Imaging of exogenous CO

In vivo time-dependent imaging experiment: DHM-CO (200 μM, 100 μL) was first injected into the hind limbs of mice. After that, CORM-3 (4 mM, 100 μL) was injected into the same location. Fluorescence images were captured at various time points.

In vivo concentration-dependent imaging experiment: DHM-CO (200 μM, 100 μL) was injected into the hind limbs of mice. Subsequently, 100 μL of CORM-3 at varying concentrations (0, 1, 2, 4, and 8 mM) were injected into the hind limbs of mice, and fluorescence imaging was conducted.

2.4.3. Imaging of endogenous CO

Mice were randomly divided into three groups: (1) Control group: Normal mice received a local injection of DHM-CO (200 μM, 100 μL) in the hind limbs, and their fluorescence images were taken at different times; (2) Experimental group: RA mice received a local injection of DHM-CO (200 μM, 100 μL) in the hind limbs, and their fluorescence images were captured at different times; and (3) Treatment group: RA mice were administered with methotrexate (MTX) (5 mg/mL, 100 μL) in the hind limbs at 24, 48, and 72 h, and DHM-CO (200 μM, 100 μL) was injected into the hind limbs before fluorescence imaging.

In vivo imaging experiments were performed using an IVIS Lumina LT Series III small animal imaging system at an excitation wavelength of 580 nm and an emission wavelength of 882 nm.

3. Results and discussion

3.1. Design principle

Fluorescent probes are increasingly becoming vital in the fields of chemical and biological sciences due to their roles in detecting molecular changes. This study introduces the design of two fluorophores, as depicted in Scheme 2.

The fluorophore HM-OH was designed based on a donor-π-acceptor (D-π-A) electronic system, where 2-methylquinoline salt serving as the electron acceptor (D) and p-tert-butylphenol acting as the electron donor (A) are connected through a double bond (π). We explored the spectral properties of HM-OH and found that it exhibited a UV-vis absorption peak at 405 nm (Fig. 1A) and a fluorescence emission peak at 474 nm, and had a Stokes shift of 69 nm. However, its fluorescence intensity was relatively low (Fig. 1B). To enhance the spectral performance of HM-OH, we modified its structure by extending its π-conjugation system. This led to the creation of a new fluorophore, DHM-OH, with an expanded Stokes shift and a red-shifted emission wavelength. The structural modification, which was based on the design principle of a donor−two-acceptor π-electron system, involved attaching another 2-methylquinoline salt molecule to the adjacent position of the hydroxyl group through a double bond. Spectroscopic performance studies revealed that DHM-OH exhibited a UV-vis absorption peak at 580 nm (Fig. 1C), a higher fluorescence intensity, a considerably red-shifted emission wavelength of 882 nm (Fig. 1D), and a significantly larger Stokes shift ($\Delta\lambda = 302$ nm). These attributes make DHM-OH highly suitable for applications requiring deep tissue penetration and reduced autofluorescence from biomolecules in both *in vitro* and *in vivo* imaging applications. Thus, DHM-OH was utilized in subsequent experiments in which its improved spectroscopic properties were exploited.

To better understand the differences between the absorption and emission wavelengths of HM-OH and DHM-OH, theoretical calculations were performed using Gaussian 16 software. The highest occupied molecular orbital (HOMO) and the lowest unoccupied molecular orbital (LUMO) energy levels of the two fluorophores were calculated (Fig. S10). The HOMO energy for HM-OH was −8.92 eV and the LUMO energy was −5.27 eV, which resulted in a HOMO-LUMO gap of 3.65 eV. Similarly, the HOMO energy for DHM-OH was −10.99 eV and the LUMO energy was −7.95 eV, which resulted in a HOMO-LUMO gap of 3.04 eV. These calculated energy gaps were well-correlated with the observed spectral properties. The smaller HOMO-LUMO gap in DHM-OH explains the red-shifts in the absorption and emission wavelengths. These theoretical insights underscore the effectiveness of the structural modification in enhancing the spectroscopic performance of the fluorophore.

3.2. Spectral characteristics of DHM-CO

To evaluate the sensing performance of DHM-CO, we analyzed its spectral response to CO using CORM-3 as a CO precursor to generate CO *in situ* [35,36]. DHM-CO exhibited a UV-vis absorption peak at 580 nm. The absorption peak reached its maximum intensity when the concentration of CORM-3 was 100 μM (Fig. 2A). As anticipated, DHM-CO was

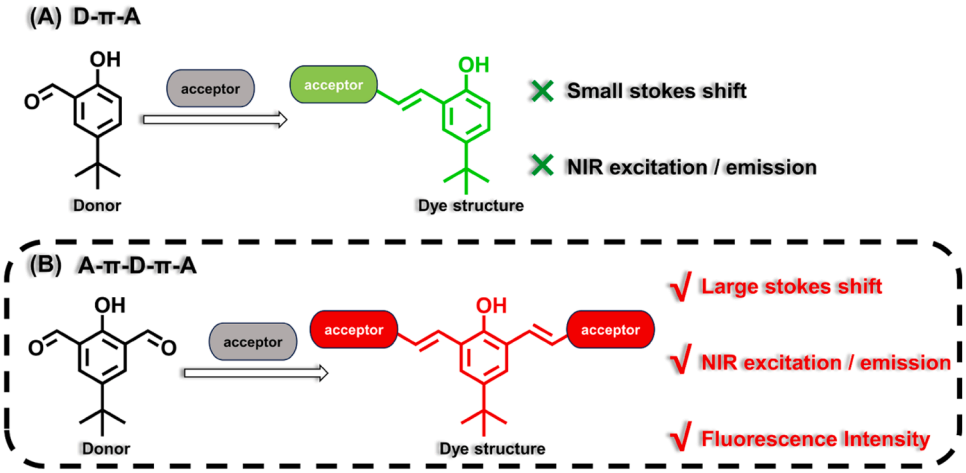

Scheme 2. *De novo* design rationale of the fluorophore.

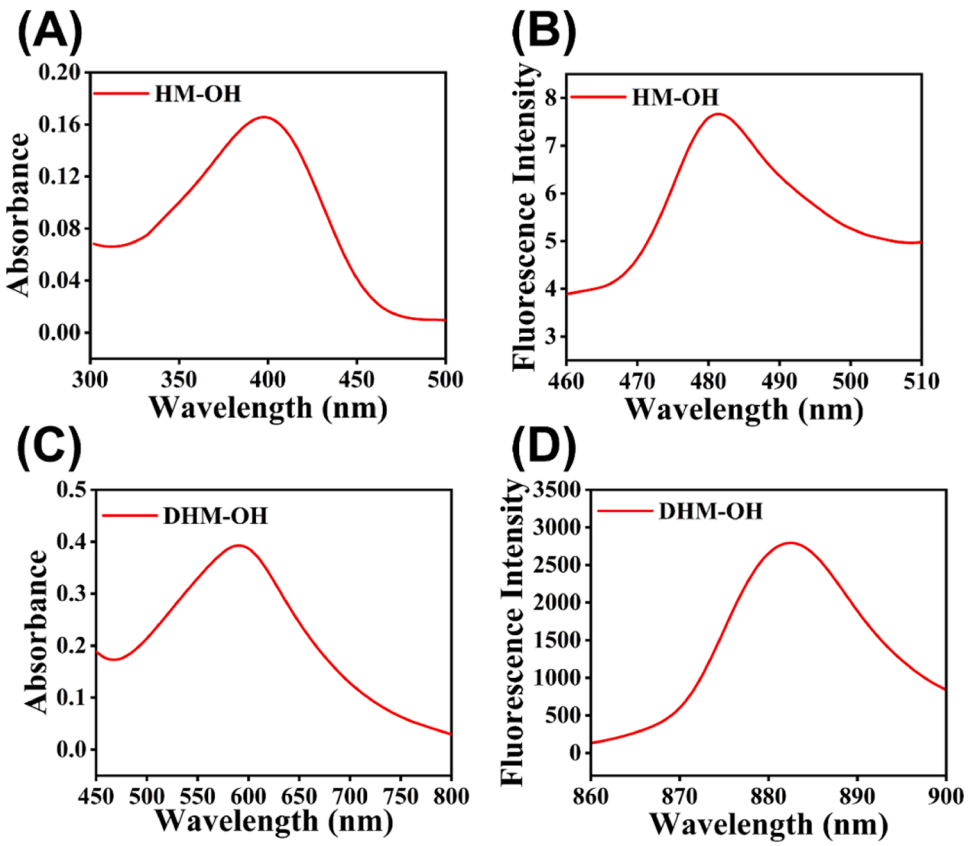

Fig. 1. (A) Fluorescence spectra of 10 μM HM-OH. (B) Absorption spectra of 10 μM HM-OH. (C) Fluorescence spectra of 10 μM DHM-OH. (D) Absorption spectra of 10 μM DHM-OH.

hypofluorescent in the absence of CO. However, upon the addition of CORM-3, a strong near-infrared fluorescence peak emerged at 882 nm (Fig. 2B). The fluorescence intensity of this peak gradually increased with the increase of CORM-3 concentrations (Fig. 2C). A linear correlation between the fluorescence intensity at 882 nm and the concentration of CORM-3 was observed ($R^2 = 0.9984$) (Fig. 2D), and the limit of detection (LOD) was determined to be 0.027 μM. The results suggest that DHM-CO is highly sensitive and exhibits a turn-on response to NIR fluorescence that enables the quantitative detection of CO. Table S1 shows the comparison of DHM-CO with other fluorescent probes, highlighting its superior excitation/emission wavelengths, limit of detection (LOD), and Stokes shift.

3.3. Response speed, stability, and selectivity of DHM-CO

The response speed of DHM-CO to CO in the presence of CORM-3 was analyzed by monitoring the fluorescence intensity at 882 nm. As shown in Fig. S11, the fluorescence intensity of DHM-CO at 882 nm increased rapidly, reaching a plateau within 40 min after the addition of CORM-3. We further evaluated the sensing performance of DHM-CO under different pH conditions. Fig. S12 demonstrates that upon the addition of CORM-3, DHM-CO exhibited a significant fluorescence enhancement at pH ranging from 6 to 9, which is indicative of its capability to detect CO under physiological conditions. Additionally, we examined the photostability of DHM-CO. Fig. S13 reveals that under 580 nm light irradiation, the fluorescence intensity of DHM-CO and the reaction system remained stable for 60 min, which is suggestive of their good photostability. The thermal stability of DHM-CO was assessed by observing the fluorescence intensity at various temperatures. Fig. S14 indicates that the fluorescence intensity of DHM-CO remained stable at temperatures between 25 °C and 45 °C, demonstrating the excellent thermal stability of DHM-CO. However, the fluorescence intensity of the reaction system increased with increasing temperatures, suggesting that the reaction rate could be accelerated at this temperature range. Fig. S15 shows that the fluorescence intensity gradually increased as the concentration of the DHM-CO probe increased, and there was a linear correlation between the fluorescence intensity and the concentration of DHM-CO ($R^2 = 0.9939$), indicating that the DHM-CO probe has good water solubility. Based on these findings and considering the physiological conditions, all subsequent experiments were performed in PBS (10 mM, pH 7.4) at 37 °C for 60 min.

In the assessment of the specificity of DHM-CO, we investigated the impact of potential interfering substances. Fig. S16 shows that spectral changes were not observed in the presence of various cations, anions, and amino acids. Only CORM-3 induced a significant fluorescence peak at 882 nm, which confirms that DHM-CO has the ability to specifically recognize CO.

In the assessment of the specificity of DHM-CO, we investigated the impact of potential interfering substances. As shown in Fig. S16, spectral changes were not observed in the presence of various cations, anions, and amino acids. To further confirm the probe's specificity for CO, we prepared a real CO solution by purging CO gas into water, following the method reported [37]. The fluorescence response of DHM-CO to the real CO solution was consistent with that observed using CORM-3, both inducing a significant fluorescence peak at 882 nm. These results confirm that DHM-CO has the ability to specifically recognize CO, regardless of its source.

3.4. Sensing mechanism of DHM-CO

The allyl ether group serves as a recognition site for CO detection. Typically, probes developed for CO detection require Pd^{2+} as a catalyst, primarily due to the Tsuji-Trost reaction [3,38,39]. However, some probes have been reported to respond to CO in the absence of Pd^{2+}.

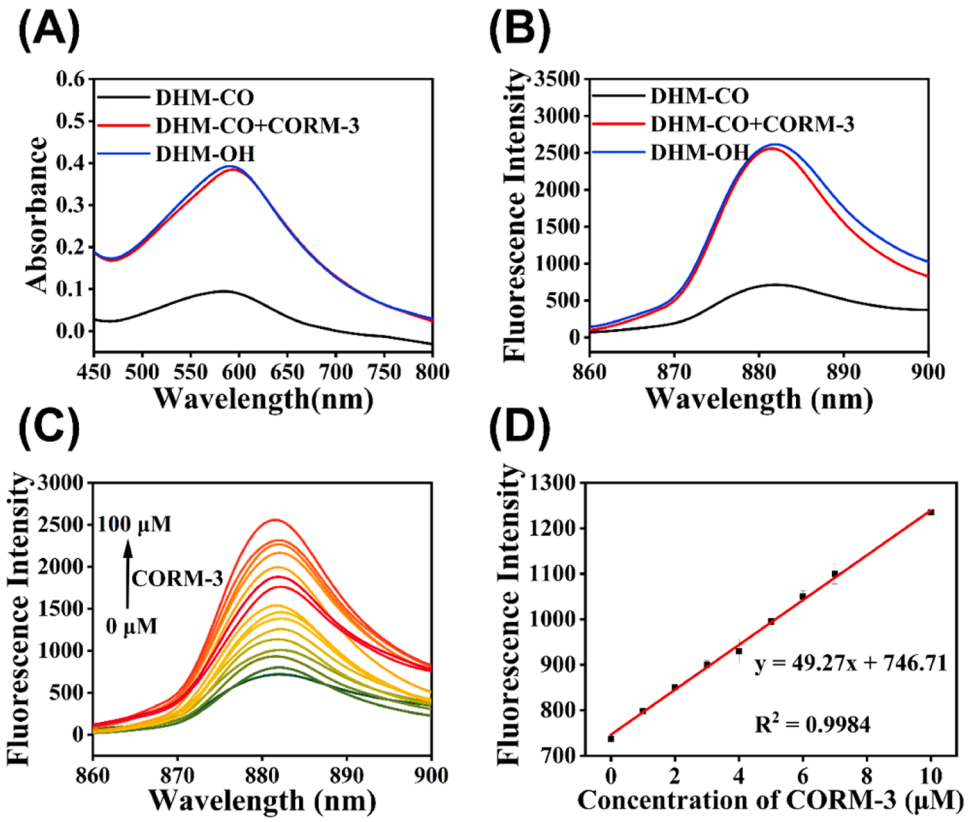

Fig. 2. (A) UV-vis absorption spectra of 10 μM DHM-CO and reaction system consisting of 10 μM DHM-CO and 100 μM CORM-3. (B) Fluorescence spectra of 10 μM DHM-CO and reaction system consisting of 10 μM DHM-CO and 100 μM CORM-3. (C) Fluorescence spectra of DHM-CO in response to CORM-3 at different concentrations (0–100 μM). (D) Linear relationship between fluorescence intensity at 882 nm of the reaction system and CORM-3 concentrations (0–10 μM).

Here, we designed a probe, DHM-CO, which does not require Pd^{2+} metal. The proposed detection mechanism is illustrated in Fig. 3. In this mechanism, the allyl ether group is first isomerized to aryl ethers by CORM-3 (CO) and subsequently hydrolyzed to DHM-OH. Additionally, numerous reports have shown that allyl groups can be cleaved by ruthenium compounds via isomerization intermediates, without the need for Pd^{2+} catalysis [30,40]. These findings support our proposed mechanism. Furthermore, in response to CORM-3, the absorption and fluorescence spectra of DHM-OH closely resembled those of DHM-CO (Fig. 2A-B). This similarity provides evidence that the probe DHM-CO was converted to DHM-OH by CORM-3. Mass spectrometry results further corroborate this mechanism. After the addition of CORM-3, the reaction system exhibited a mass peak at m/z 257.1482 (Fig. S17), which is consistent with that of DHM-OH (m/z 257.1487) (Fig. S6).

3.5. *Imaging of CO in cells*

For cellular imaging applications of fluorescent probes, biocompatibility is critical. Prior to cell imaging, we evaluated the cytotoxicity of DHM-CO using a CCK-8 assay. After 24 h of incubation with DHM-CO,

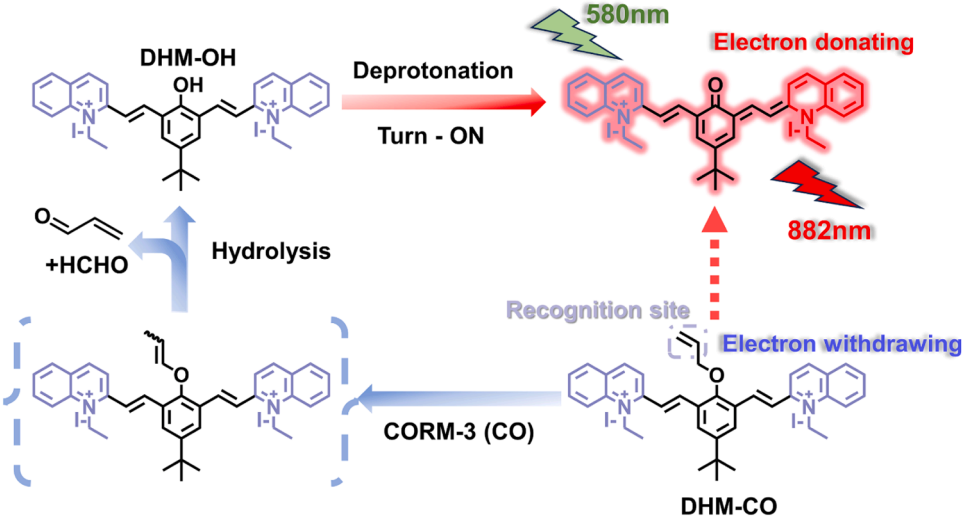

Fig. 3. The proposed CO-sensing mechanism of DHM-CO.

even at low concentrations (0, 10, 20, 40, and 50 μM), the cell viability remained above 90 % (Fig. S18). This indicates that DHM-CO possesses good biocompatibility. Additionally, we assessed the biocompatibility of DHM-CO using a hemolysis assay (Fig. S19). The results showed that after incubation with DHM-CO at concentrations up to 50 μM for 3 h, the hemolysis rate of erythrocytes was less than 3 %. This shows that DHM-CO is suitable for endogenous CO imaging in living cells.

Fluorescence imaging of DHM-CO in A549 cells was subsequently performed. Upon the addition of CORM-3 (50 μM), the intracellular fluorescence intensity increased over time (Fig. 4A). Specifically, DHM-CO (10 μM) showed a rapid increase in fluorescence intensity during the first 60 min, which then remained constant during the following 30 min. Consequently, DHM-CO was incubated with cells for 60 min in the subsequent imaging experiments. We investigated the correlation between DHM-CO fluorescence and CO concentration (Fig. 4B). After incubating A549 cells with DHM-CO (10 μM) for 60 min, fluorescence in the red channel was not observed, indicating that the CO level in DHM-CO-treated cells was too low and thus undetectable. However, by incubating the cells with CORM-3 at varying concentrations (10, 25, 50, and 100 μM) for 60 min, a gradual increase in the fluorescence intensity in the red channel was observed, and the increase correlated with the concentration of CORM-3. This suggests that DHM-CO can effectively image exogenous CO in live A549 cells.

CO is a gaseous signaling molecule that can be produced endogenously. It plays a crucial role in various physiological processes. Abnormal CO levels are associated with the occurrence of several diseases in living cells. Therefore, we employed DHM-CO to monitor CO fluctuations in A549 cells. Research has shown that lipopolysaccharide (LPS) can activate various intracellular pathways, thereby altering the expression of a variety of inflammatory mediators and enabling endogenous CO production [41]. Consequently, LPS was used as a promoter of CO production, while penicillin G sodium salt (PG) was employed as an inhibitor. As shown in Fig. 4C, A549 cells did not exhibit red channel fluorescence despite the incubation with DHM-CO for 60 min. However, upon inducing inflammation in the cells with LPS (0.1 mg/mL, 200 μL, 3 h), a significant enhancement in the red-channel fluorescence was observed. After that, cellular inflammation was treated with PG, which is a commonly used anti-inflammatory agent known to reduce endogenous CO production by alleviating cellular oxidative stress. It was found that the fluorescence intensity of cells treated with PG (0.1 mg/mL, 200 μL, 3 h) decreased significantly, indicating a substantial reduction in CO levels. The average fluorescence intensities are presented in Fig. 4C. These results suggest that endogenous CO levels are elevated in inflammatory cells and that DHM-CO can effectively monitor the CO levels in living cells.

3.6. *Imaging of CO in vivo*

Given that DHM-CO demonstrated excellent *in vitro* CO imaging capability, we subsequently utilized it for exogenous CO imaging in the hind limbs of living mice (Fig. 5A). As depicted in Fig. 5B, DHM-CO (200 μM, 100 μL) was injected into the hind limbs of normal mice, followed by CORM-3 (4 mM, 100 μL). The fluorescence signals in the hind limbs of the mice significantly increased over time, reaching a maximum value at 20 min (Fig. 6B). We further examined the effects of different CORM-3 concentrations on DHM-CO fluorescence signals. DHM-CO (200 μM, 100 μL) was injected into the hind limbs of mice, followed by CORM-3 at varying concentrations (0, 1, 2, 4, and 8 mM, 100 μL). The fluorescence signals were notably enhanced as the concentration of CORM-3 increased (Fig. 5C). The quantitative fluorescence intensity data are shown in Fig. S20. These results indicate that DHM-CO can rapidly and sensitively detect exogenous CO in living animals.

Next, we explored CO-mediated inflammation in living mice with rheumatoid arthritis (RA) using DHM-CO (Fig. 6A). A rheumatoid

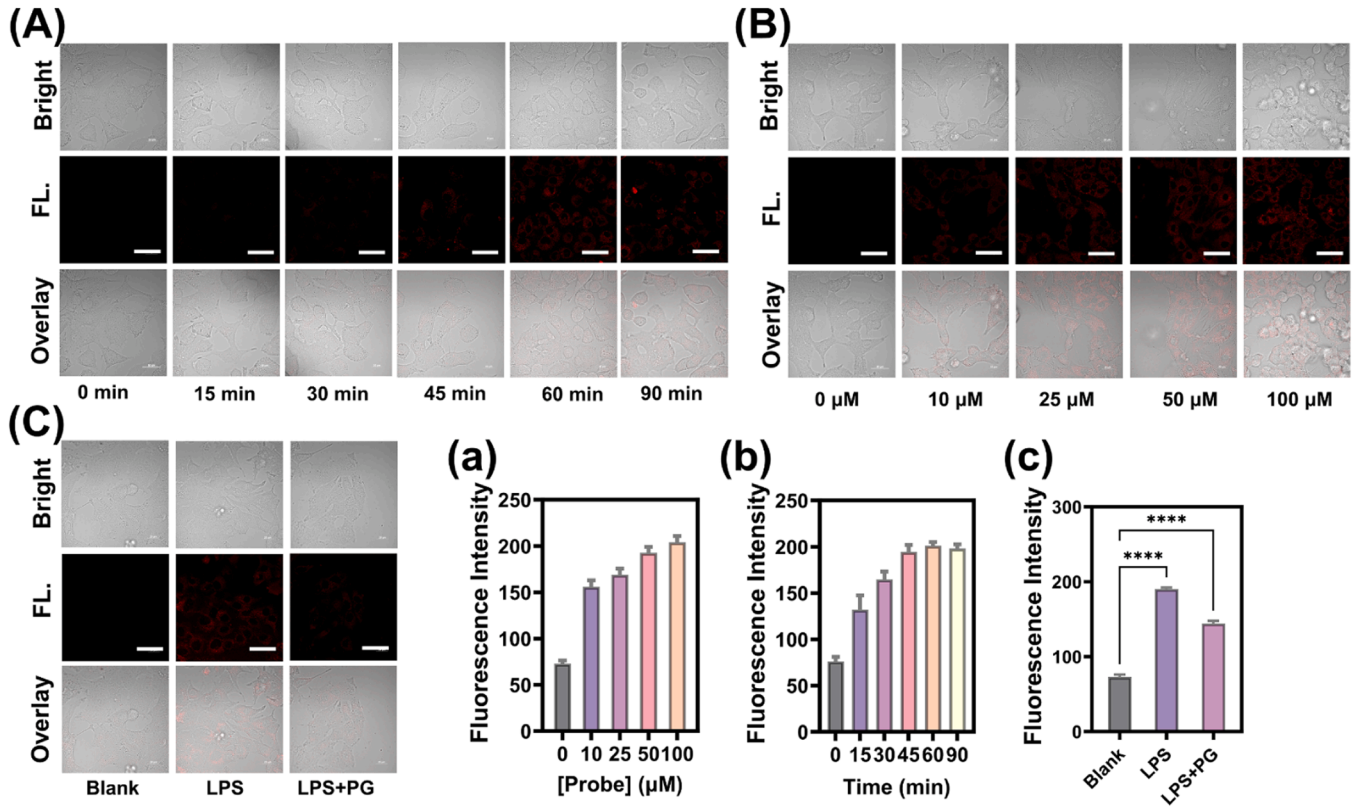

Fig. 4. (A) Fluorescence intensity of A549 cells after incubating with probe DHM-CO and CORM-3 (50 μM). Scale bar = 20 μm. (a) Mean fluorescence intensity of cells in (A). (B) Variation of intracellular fluorescence intensity with CO concentration. Scale bar = 20 μm. (b) Mean fluorescence intensity of cells in (B). (C) Fluorescence intensity of endogenous CO in A549 cells. Scale bar = 20 μm. (c) Mean fluorescence intensity of cells in (C).

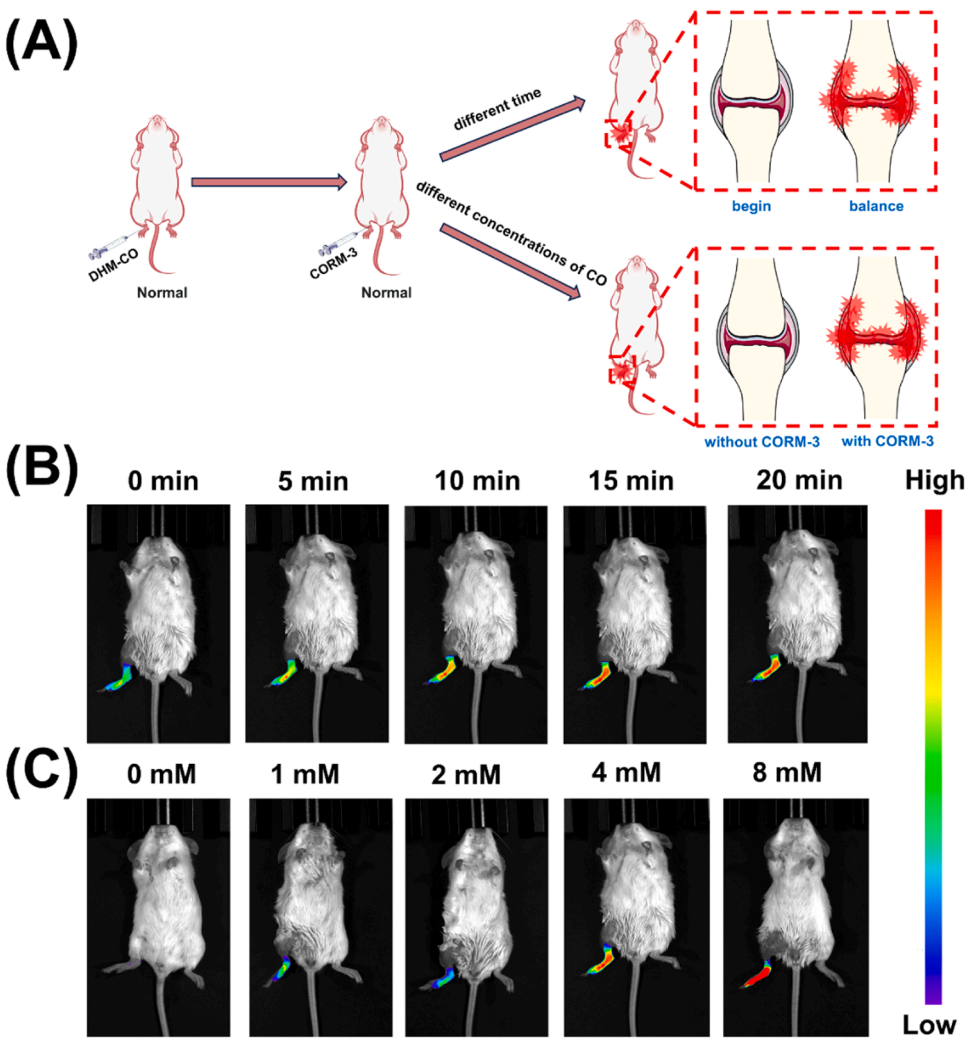

Fig. 5. (A) Diagram showing time-dependent imaging of the hind limb of healthy mice injected with 4 mM CORM-3 (100 μL) after being *in situ* injected with probe DHM-CO (200 μM, 100 μL), and concentration-dependent imaging of the mice injected with different concentrations of CORM-3 (0, 1, 2, 4, and 8 mM, 100 μL). (B) Time-dependent images of healthy mice *in situ* injected with probe DHM-CO (200 μM, 100 μL), followed by 4 mM CORM-3 (100 μL). (C) Concentration-dependent images of healthy mice *in situ* injected with probe DHM-CO (200 μM, 100 μL), followed by different concentrations of CORM-3 (0, 1, 2, 4, and 8 mM, 100 μL).

arthritis mouse model was established by administering λ-carrageenan (5 mg/mL, 50 μL) into the hind limbs every three days for two consecutive weeks (Fig. S21) [42,43]. DHM-CO (200 μM, 100 μL) was then injected into the hind limbs of the mice. As shown in Fig. 6B, due to increased CO levels caused by λ-carrageenan-induced RA, prominent fluorescence emission from the hind limbs was observed, and the emission gradually intensified over time, peaking at 12 min. In contrast, significant fluorescence signals were not detected in the hind limbs of normal mice (Fig. 6C). The quantitative fluorescence intensity data are shown in Fig. S22. These findings suggest that CO is a critical mediator of RA in mice and that DHM-CO can effectively monitor endogenous CO production in mice with RA. Therefore, by tracking CO production, DHM-CO could be utilized to diagnose RA. Additionally, this fluorescent probe can be employed for the pharmacodynamic evaluation of anti-inflammatory drugs. We investigated the capacity of DHM-CO to assess the efficacy of anti-RA drugs (Fig. 6A). RA in the hind limbs of mice was induced by λ-carrageenan. Methotrexate (MTX) (100 μM, 100 μL), a standard RA treatment drug, was locally injected into the hind limbs of mice in the treatment group. DHM-CO (200 μM, 100 μL) was injected into the hind limbs of mice after 24, 48, and 72 h of treatment. As illustrated in Fig. 6D, the fluorescence emission from the hind limbs notably declined as the treatment period progressed, an indication that MTX can effectively treat RA. The quantitative fluorescence intensity data are shown in Fig. S23. These results suggest that DHM-CO can be used as an effective fluorescent probe to evaluate the responses to RA treatment by monitoring changes in CO levels.

4. Conclusions

In summary, we designed and synthesized a new fluorescent probe, DHM-CO, for the detection of CO-mediated rheumatoid arthritis. In the presence of CO, but without Pt^{2+}, the absorption and emission spectra of the probe significantly changed due to the cleavage of allyl groups by ruthenium compounds (via an isomerization intermediate). The probe DHM-CO has several advantages, including a long emission wavelength, a large Stokes shift, high sensitivity, a fast fluorescence "OFF-ON" response, and biocompatibility. Notably, DHM-CO was successfully used for real-time monitoring of both endogenous and exogenous CO in cells. Importantly, CO-mediated RA inflammatory response and RA therapeutic response were successfully demonstrated in living mice. This new fluorescent probe, DHM-CO, is a promising tool for studying other CO-mediated biological processes and offer valuable insights for the diagnosis and treatment of CO-related diseases.

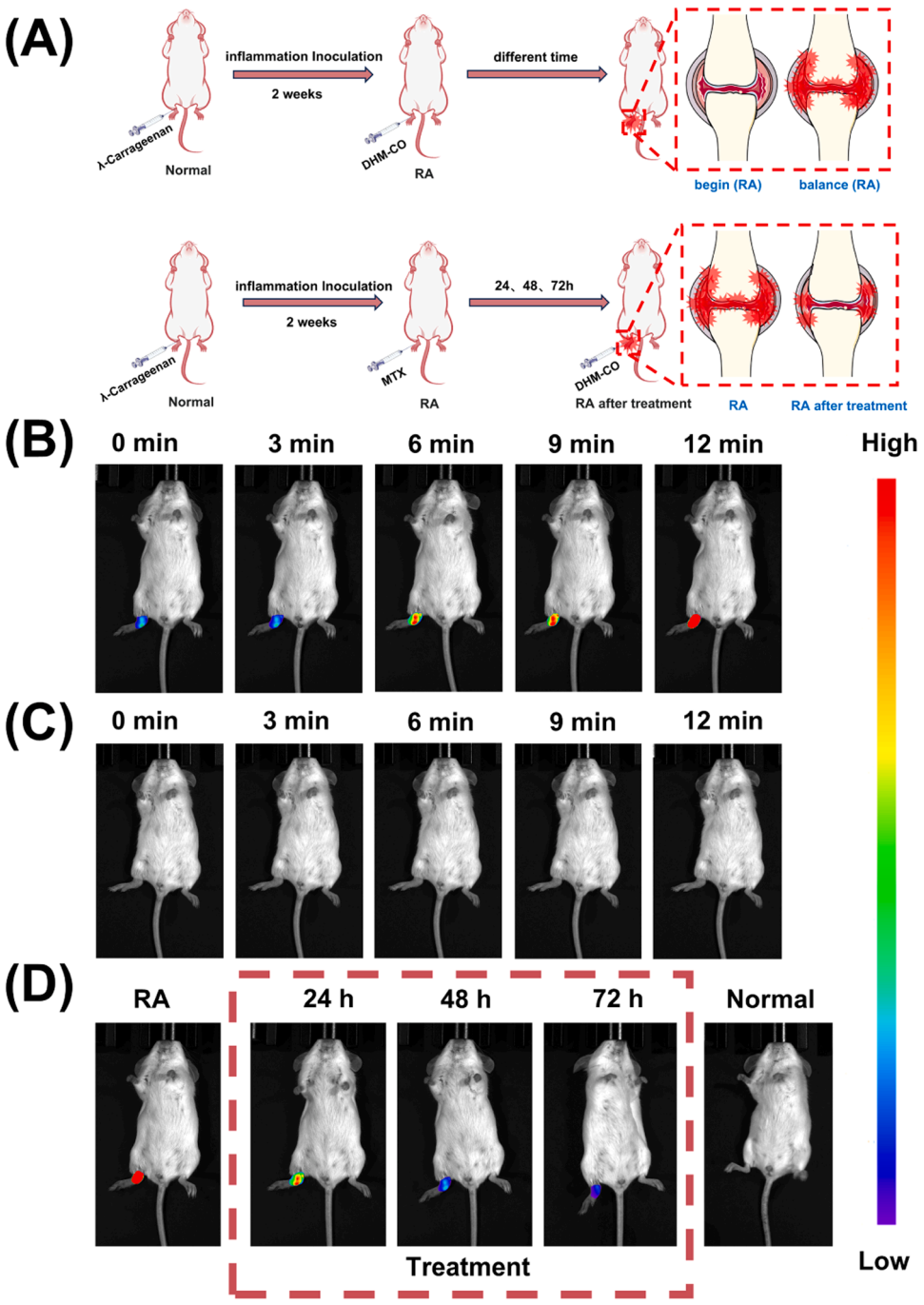

Fig. 6. (A) Illustration demonstrating the time-dependent imaging of the hind limbs of rheumatoid arthritis mice in situ injected with probe DHM-CO (200 μM, 100 μL). The figure also depicts the fluorescence imaging of rheumatoid arthritis mice following drug treatment. (B) Time-dependent imaging of probe DHM-CO (200 μM, 100 μL) in rheumatoid arthritis mice. (C) Time-dependent imaging of healthy mice *in situ* injected with probe DHM-CO (200 μM, 100 μL). (D) Fluorescence imaging of mice receiving the drug for rheumatoid arthritis treatment after *in situ* injection with probe DHM-CO (200 μM, 100 μL).

CRediT authorship contribution statement

Wenping Dong: Writing – original draft, Validation, Investigation, Data curation, Conceptualization. **Mo Ma:** Investigation, Data curation. **Jingkang Li:** Investigation, Data curation. **Dejiang Gao:** Software, Formal analysis. **Pinyi Ma:** Writing – review & editing, Project administration, Data curation, Conceptualization. **Daqian Song:** Supervision, Resources, Project administration, Funding acquisition.

Declaration of Competing Interest

The authors declare that they have no known competing financial interests or personal relationships that could have appeared to influence the work reported in this paper.

Acknowledgments

This work was supported by the National Natural Science Foundation of China (22004046 and 22074052) and the Science and Technology Developing Foundation of Jilin Province of China (20240404044ZP).

Appendix A. Supporting information

Supplementary data associated with this article can be found in the online version at doi:10.1016/j.snb.2025.137401.

Data availability

Data will be made available on request.

References

[1] L. Yuan, W. Lin, L. Tan, K. Zheng, W. Huang, Lighting up carbon monoxide: fluorescent probes for monitoring CO in living cells, Angew. Chem. Int. Ed. 52 (2012) 1628–1630.
[2] D. Stucki, W. Stahl, Carbon monoxide – beyond toxicity? Toxicol. Lett. 333 (2020) 251–260.
[3] S. Feng, D. Liu, W. Feng, G. Feng, Allyl fluorescein ethers as promising fluorescent probes for carbon monoxide imaging in living cells, Anal. Chem. 89 (2017) 3754–3760.
[4] H. Kitagishi, S. Minegishi, A. Yumura, S. Negi, S. Taketani, Y. Amagase, et al., Feedback response to selective depletion of endogenous carbon monoxide in the blood, J. Am. Chem. Soc. 138 (2016) 5417–5425.
[5] E. Zhou, S. Gong, Q. Xia, G. Feng, In vivo imaging and tracking carbon monoxide-releasing molecule-3 with an NIR fluorescent probe, ACS Sens. 6 (2021) 1312–1320.
[6] K. Liu, X. Kong, Y. Ma, W. Lin, Rational design of a robust fluorescent probe for the detection of endogenous carbon monoxide in living zebrafish embryos and mouse tissue, Angew. Chem. Int. Ed. 56 (2017) 13489–13492.
[7] J.A. Sparks, Rheumatoid arthritis, Ann. Intern. Med. 170 (2019) Itc1–Itc15.
[8] D. Aletaha, J.S. Smolen, Diagnosis and management of rheumatoid arthritis, JAMA 320 (2018) 1360.
[9] J.S. Smolen, D. Aletaha, I.B. McInnes, Rheumatoid arthritis, Lancet 388 (2016) 2023–2038.
[10] Sy Kawashiri, T. Suzuki, Y. Nakashima, Y. Horai, A. Okada, A. Nishino, et al., Synovial inflammation assessed by ultrasonography correlates with MRI-proven osteitis in patients with rheumatoid arthritis, Rheumatology 53 (2014) 1452–1456.
[11] Y. Liu, L. Chen, Z. Chen, M. Liu, X. Li, Y. Kou, et al., Multifunctional Janus nanoplatform for efficiently synergistic theranostics of rheumatoid arthritis, ACS Nano 17 (2023) 8167–8182.
[12] Y.-J. Lin, M. Anzaghe, S. Schülke, Update on the pathomechanism, diagnosis, and treatment options for rheumatoid arthritis, Cells 9 (2020) 880.
[13] S. Zhou, W. Mao, Y. Su, X. Zheng, W. Qian, M. Shen, et al., Identification of TUL01101: a novel potent and selective JAK1 inhibitor for the treatment of rheumatoid arthritis, J. Med. Chem. 65 (2022) 16716–16740.
[14] H. Kobayashi, M. Takeno, T. Saito, Y. Takeda, Y. Kirino, K. Noyori, et al., Regulatory role of heme oxygenase 1 in inflammation of rheumatoid arthritis, Arthritis Rheum. 54 (2006) 1132–1142.
[15] T.-l Yuan, J. Chen, Y.-l Tong, Y. Zhang, Y.-y Liu, J.C.-C. Wei, et al., Serum heme oxygenase-1 and BMP-7 are potential biomarkers for bone metabolism in patients with rheumatoid arthritis and ankylosing spondylitis, Biomed. Res. Int. 2016 (2016) 1–7.
[16] R.R. Mititelu, R. Pădureanu, M. Băcănoiu, V. Pădureanu, A.O. Docea, D. Calina, et al., Inflammatory and oxidative stress markers—mirror tools in rheumatoid arthritis, Biomedicines 8 (2020) 125.
[17] A.-R. Phull, B. Nasir, Iu Haq, S.J. Kim, Oxidative stress, consequences and ROS mediated cellular signaling in rheumatoid arthritis, Chem. Biol. Interact. 281 (2018) 121–136.
[18] J. Wang, C. Li, Q. Chen, H. Li, L. Zhou, X. Jiang, et al., An easily available ratiometric reaction-based AIE probe for carbon monoxide light-up imaging, Anal. Chem. 91 (2019) 9388–9392.
[19] S. Huang, X. Liu, J. Hou, M. Liu, T. Luo, X. Huang, et al., A novel red AIE fluorescent probe for ratiometric detection of carbon monoxide in vitro and in vivo, J. Mater. Chem. B 11 (2023) 3871–3876.
[20] G. Gan, T. Ma, G. Zhang, K. He, J. Hu, Luminescent probes for detecting and bioimaging of nitric oxide and carbon monoxide, TrAC Trends Anal. Chem. 168 (2023) 117340.
[21] J. Zhao, X. Chen, K.-H. Ho, C. Cai, C.-W. Li, M. Yang, et al., Nanotechnology for diagnosis and therapy of rheumatoid arthritis: evolution towards theranostic approaches, Chin. Chem. Lett. 32 (2021) 66–86.
[22] H. Xiong, H. Zuo, Y. Yan, G. Occhialini, K. Zhou, Y. Wan, et al., High-contrast fluorescence detection of metastatic breast cancer including bone and liver micrometastases via size-controlled pH-activatable water-soluble probes, Adv. Mater. 29 (2017) 1700131.
[23] H. Li, D. Kim, Q. Yao, H. Ge, J. Chung, J. Fan, et al., Activity-based NIR enzyme fluorescent probes for the diagnosis of tumors and image-guided surgery, Angew. Chem. Int. Ed. 60 (2021) 17268–17289.
[24] M. Yang, J. Fan, J. Du, X. Peng, Small-molecule fluorescent probes for imaging gaseous signaling molecules: current progress and future implications, Chem. Sci. 11 (2020) 5127–5141.
[25] D. Wu, A.C. Sedgwick, T. Gunnlaugsson, E.U. Akkaya, J. Yoon, T.D. James, Fluorescent chemosensors: the past, present and future, Chem. Soc. Rev. 46 (2017) 7105–7123.
[26] C. Ding, T. Ren, Near infrared fluorescent probes for detecting and imaging active small molecules, Coord. Chem. Rev. 482 (2023) 215080.
[27] J. Zhan, W. Song, E. Ge, L. Dai, W. Lin, Reversible fluorescent probes for biological dynamic imaging: current advances and future prospects, Coord. Chem. Rev. 493 (2023) 215321.
[28] S. Han, Y. Zeng, Y. Li, H. Li, L. Yang, X. Ren, et al., Carbon monoxide: a second biomarker to couple with viscosity for the construction of "dual-locked" near-infrared fluorescent probes for accurately diagnosing non-alcoholic fatty liver disease, Anal. Chem. 95 (2023) 18619–18628.
[29] Y.-S. Chen, B.-Z. Zhou, F.-T. Liu, H.-Y. Yu, J.-Y. Miao, B.-X. Zhao, et al., A novel fluorescent probe for ultra-fast detection of CORM-3 and spatiotemporal multi-organelle targeting, Sens. Actuators B Chem. 399 (2024) 134824.
[30] A. Sarkar, S. Hansda, T. Dutta, S. Ghoshal, S. Mukhopadhyay, P. Sarkar, et al., Endoplasmic reticulum-targeted fluorescent probes for metal-free tracking of carbon monoxide in living cells, Sens. Actuators B Chem. 393 (2023) 134150.
[31] X.-Y. Zhu, H.-W. Yao, Y.-J. Fu, X.-F. Guo, H. Wang, Effect of substituents on Stokes shift of BODIPY and its application in designing bioimaging probes, Anal. Chim. Acta 1048 (2019) 194–203.
[32] M. Jiang, X. Gu, J.W.Y. Lam, Y. Zhang, R.T.K. Kwok, K.S. Wong, et al., Two-photon AIE bio-probe with large Stokes shift for specific imaging of lipid droplets, Chem. Sci. 8 (2017) 5440–5446.
[33] Q. An, S. Su, L. Chai, Y. Wang, X. Wang, X. Li, et al., Imaging of peroxynitrite in mitochondria by a near-infrared fluorescent probe with a large Stokes shift, Talanta 253 (2023) 124073.
[34] W.-L. Fang, Z.-Y. Liang, X.-F. Guo, H. Wang, A D-π-A-based near-infrared fluorescent probe with large Stokes shift for the detection of cysteine in vivo, Talanta 268 (2024) 125354.
[35] Y. Shin, K. Whang, J.H. Hwang, Y. Jo, J.-W. Choi, J. Park, et al., Sensitive and direct optical monitoring of release and cellular uptake of aqueous CO from CO-releasing molecules, Anal. Chem. 93 (2021) 9927–9932.
[36] B. Zhu, X. Xing, J. Kim, H. Rha, C. Liu, Q. Zhang, et al., Endogenous CO imaging in bacterial pneumonia with a NIR fluorescent probe, Biomaterials 304 (2024) 122419.
[37] J. Wang, J. Karpus, B.S. Zhao, Z. Luo, P.R. Chen, C. He, A selective fluorescent probe for carbon monoxide imaging in living cells, Angew. Chem. Int. Ed. 51 (2012) 9652–9656.
[38] W. Feng, G. Feng, A readily available colorimetric and near-infrared fluorescent turn-on probe for detection of carbon monoxide in living cells and animals, Sens. Actuators B Chem. 255 (2018) 2314–2320.
[39] Z. Zheng, S. Feng, S. Gong, G. Feng, Golgi-targetable fluorescent probe for ratiometric imaging of CO in cells and zebrafish, Sens. Actuators B Chem. 347 (2021) 130631.
[40] S. Gong, E. Zhou, Y. Liu, Z. Gui, G. Feng, A Pd2+-free near-infrared fluorescent probe based on allyl ether isomerization for tracking CORM-3 with high contrast imaging in living systems, Anal. Chem. 94 (2022) 2042–2047.
[41] W. Jing, C. Liu, C. Su, L. Liu, P. Chen, X. Li, et al., Role of reactive oxygen species and mitochondrial damage in rheumatoid arthritis and targeted drugs, Front. Immunol. 14 (2023) 1107670.
[42] X.-B. Wang, H.-J. Li, Q. Li, Y. Ding, C. Hu, Y.-C. Wu, A specifically triggered turn-on fluorescent probe platform and its visual imaging of HClO in cells, arthritis and tumors, J. Hazard. Mater. 427 (2022) 127874.
[43] W. Qu, R. Tian, B. Yang, T. Guo, Z. Wu, Y. Li, et al., Dual-channel/localization single-molecule fluorescence probe for monitoring ATP and HOCl in early diagnosis and therapy of rheumatoid arthritis, Anal. Chem. 96 (2024) 5428–5436.

Wenping Dong is currently a master degree student in College of Chemistry, Jilin University. Her interest is spectral analysis.

Mo Ma is currently a PhD student in School of Pharmacy, Jilin University. His interest is spectral analysis.

Jingkang Li is currently a PhD student in College of Chemistry, Jilin University. His interest is spectral analysis.

Dejiang Gao gained his doctor's degree from College of Chemistry, Jilin University in 2008 and he is a professor in that school. His research areas is spectral analysis.

Pinyi Ma gained his doctor's degree from College of Chemistry, Jilin University in 2017 and he is an associate professor in that school. His research area is spectral analysis.

Daqian Song gained his doctor's degree from College of Chemistry, Jilin University in 2003 and he is a professor in that school. His research areas are spectral and chromatography analysis.